

Finite Sample Thickness Effects on Elasticity Determination Using Atomic Force Microscopy

Boris B. Akhremitchev and Gilbert C. Walker*

Department of Chemistry, University of Pittsburgh, Pittsburgh, Pennsylvania 15260

Received May 15, 1998. In Final Form: April 28, 1999

Finite sample thickness effects on material elasticity measurements made using an atomic force microscope have been calculated. The model includes an elastic layer on an elastic foundation and simulates sample indentation under an applied load. Rigid axisymmetric tips with conical, paraboloidal, and hyperboloidal profiles are considered. The results show that a common approach to estimating elastic moduli from force–displacement curves can lead to a significant error that depends on the units of measurement. A method to unambiguously estimate and correct this error is proposed. In addition, it is shown that elasticity estimates for monolayer thick samples using the force–modulation technique can contain a substantial, sample thickness-dependent error. Local thickness variations can result in misleading contrast in force–modulation images for samples that are several nanometers thick.

Atomic Force Microscopy (AFM) measurements are often made on thin film samples with thicknesses that range from a few nanometers to micrometers. Quantitative elasticity measurements using AFM are usually interpreted assuming a semiinfinite sample geometry.^{1–12} In this paper, we model the effect of the substrate on elasticity measurements made on thin films. This effect is particularly important when mapping the Young modulus of samples that exhibit inhomogeneous thickness variations¹³ and when testing the breakdown of macroscopic models of elasticity. We use Sneddon mechanics to model the elastic deformation.^{14,15} The modulus of elasticity for typical polymeric and biological samples is several orders of magnitude smaller than the modulus of the underlying hard substrate.¹ We calculate sample indentation by considering a rigid axisymmetric tip under an applied load, and we report that a significant error can arise from a common assumption of infinite sample thickness. The influence of the substrate on the elastic reaction of thin films was considered by Kim for nanoindentation experiments using a pyramidal indenter.¹⁶ For small indentation depths, the pyramidal indenter model gives a large error

in the evaluated elastic modulus;¹⁷ therefore we consider conical, paraboloidal, and hyperboloidal tip profiles. The numerical calculations provided here can be used to correct the elastic modulus obtained under the assumption of a semiinfinite sample geometry. The layer and the substrate deformations are considered to be purely elastic; we do not consider viscoelastic and plastic deformation effects. The purely plastic deformation of a bilayer was considered by Felder and co-workers.¹⁸

Presently the most common techniques for measuring elasticity with high spatial resolution are indentation measurements^{1,2,6–12} and force–modulation^{3–5} experiments performed using AFM. These measurements are interpreted using a model that includes a paraboloidal or conical tip that elastically indents a half-space sample. However, sharp AFM tips often have a conical shape with a rounded apex (manufacturers typically specify a 10–100 nm radius of curvature). A hyperboloidal tip profile simulates this shape. Figure 1a shows the tip shapes; Figure 1b shows the indentation geometry and introduces variables and parameters. Different tip profiles illustrate the role of the indentation geometry in estimating the elastic modulus of thin samples.

The elastic modulus of a semiinfinite sample can be estimated using load–indentation dependencies as described by Sneddon.¹⁴

$$F = \frac{2E \tan(\alpha)}{\pi(1 - \sigma^2)} \delta^2 \quad (1a)$$

$$F = \frac{4E\sqrt{R}}{3(1 - \sigma^2)} \delta^{3/2} \quad (1b)$$

$$\left. \begin{aligned} \delta &= \frac{a^2}{2R\xi} \left[\frac{\pi}{2} + \arctan\left(\frac{1}{2\xi} - \frac{\xi}{2}\right) \right] \\ F &= \frac{Ea^3}{(1 - \sigma^2)R} \left[\xi^2 + \frac{\xi}{2} (1 - \xi^2) \left[\frac{\pi}{2} + \arctan\left(\frac{1}{2\xi} - \frac{\xi}{2}\right) \right] \right] \\ \text{where } \xi &= \frac{R \cot(\alpha)}{a} \end{aligned} \right\} \quad (1c)$$

Equations 1a–c correspond to conical, paraboloidal, and hyperboloidal shapes of revolution, respectively. Here F is load, δ is indentation, a is contact area radius, R is tip

* To whom correspondence should be addressed.

(1) Heuberger, M.; Dietler, G.; Schlapbach, L. *Nanotechnology* **1994**, *5*, 12–23.

(2) Tao, N. J.; Lindsay, S. M.; Lees, S. *Biophys. J.* **1992**, *63*, 1165–1169.

(3) Radmacher, M.; Tillmann, R. W.; Fritz, M.; Gaub, H. E. *Science* **1992**, *257*, 1900–1905.

(4) Akari, S. O.; van der Vegte, E. M.; Grim, P. C. M.; Belder, G. F.; Koutsos, V.; ten Brinke, G.; Hadziioannou, G. *Appl. Phys. Lett.* **1994**, *65*, 1915–1917.

(5) Overney, R. M.; Meyer, E.; Frommer, J.; Güntherodt, H.-J.; Fujihira, M.; Takano, H.; Gotoh, Y. *Langmuir* **1994**, *10*, 1281–1286.

(6) Radmacher, M.; Fritz, M.; Cleveland J. P.; Walters, D. A.; Hansma, P. K. *Langmuir* **1994**, *10*, 3809–3814.

(7) Radmacher, M.; Fritz, M.; Hansma, H. G.; Hansma, P. K. *Biophys. J.* **1995**, *69*, 264–270.

(8) Radmacher, M.; Fritz, M.; Kacher, C. M.; Cleveland J. P.; Hansma, P. K. *Biophys. J.* **1996**, *70*, 556–567.

(9) Nie, H.-Y.; Motomatsu, M.; Mizutani, W.; Tokumoto, H. *Thin Solid Films* **1996**, *273*, 143–148.

(10) Hansma, H. G.; Kim, K. J.; Laney, D. E.; Garcia, R. A.; Argaman, M.; Allen, M. J.; Parsons, S. M. *J. Struct. Biol.* **1997**, *119*, 99–108.

(11) Magonov, S. N.; Reneker, D. H. *Annu. Rev. Mater. Sci.* **1997**, *27*, 175–222.

(12) Hofmann, U. G.; Rotchs, C.; Parak, W. J.; Radmacher, M. *J. Struct. Biol.* **1997**, *119*, 84–91.

(13) Akhremitchev, B. B.; Mohny, B. K.; Marra, K. G.; Chapman, T. M.; Walker, G. C. *Langmuir* **1998**, *14*, 3976–3982.

(14) Sneddon, I. N. *Int. J. Eng. Sci.* **1965**, *3*, 47–57.

(15) Heuberger, M.; Dietler, G.; Schlapbach, L. *J. Vac. Sci. Technol. B* **1996**, *14*, 1250–1254.

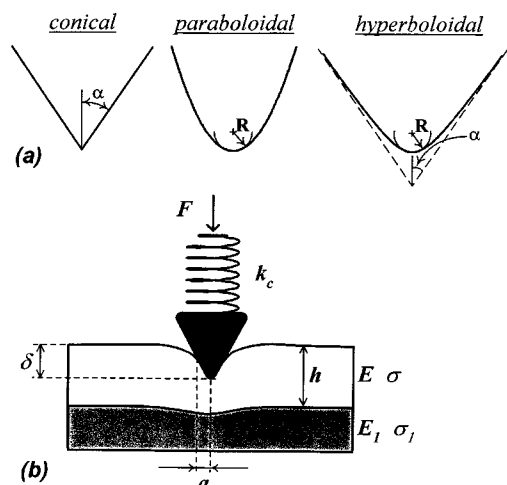


Figure 1. (a) AFM tip profiles considered in this paper: α , semivertical angle; R , radius of curvature of the tip apex. (b) Geometry of sample indentation: δ , indentation; F , load; a , contact area radius; k_c , cantilever spring constant; h , sample layer thickness; E , E_1 , σ , σ_1 , Young moduli and Poisson ratios of the sample layer and substrate, respectively.

radius of curvature, α is tip semivertical angle, E is Young modulus, and σ is Poisson ratio, as illustrated in Figure 1. From eqs 1a,b it may be seen that in a linear fit in $\log(F)$ vs $\log(\delta)$ coordinates, the intercept is related to the Young modulus:

$$\log(F) = \log\left(\frac{2E \tan(\alpha)}{\pi(1 - \sigma^2)}\right) + 2 \log(\delta) \quad (2a)$$

$$\log(F) = \log\left(\frac{4E\sqrt{R}}{3(1 - \sigma^2)}\right) + \frac{3}{2} \log(\delta) \quad (2b)$$

Using eq 2a (conical shape) for tips with rounded apices results in considerable error. For example, to estimate the Young modulus within a factor of 2 (using a hyperboloidal tip with a 20° semivertical angle and a 10 nm radius of curvature, according to eqs 1c) the maximum indentation should be larger than $2.5 \mu\text{m}$. On the other hand, eq 2b gives a factor-of-two error for indentations that are ca. 400 nm using the same parameters. This is anticipated, since eqs 1c transform into eq 1a when $R \ll a \tan(\alpha)$ and into eq 1b when $a \ll R \cot(\alpha)$.

It is intuitively clear that when a soft sample rests on a hard foundation, the tip should start to "feel" substructure when the radius of contact area is comparable to the sample thickness.¹⁹ This gives nonlinear force-indentation curves in logarithmic coordinates. Figure 2 explicitly illustrates this effect. The figure shows the indentation of a ~ 30 nm thick spin-cast sample of *coblock*(polystyrene-poly(vinylpyridine)) polymer on a microscope coverslip substrate.²⁰ The tip radius was approximately 60 nm.²⁰

(16) Kim, M. T. *Thin Solid Films* **1996**, *283*, 12–16.

(17) Chizhik, S. A.; Huang, Z.; Gorbunov, V. V.; Myshkin N. K.; Tsukruk V. V. *Langmuir* **1998**, *14*, 2606–2609.

(18) Leboviev, D.; Gilormini, P.; Felder, E. *J. Phys. D: Appl. Phys.* **1985**, *18*, 199–210. Pivin, J. C.; Leboviev, D.; Pollock, H. M.; Felder, E. *J. Phys. D: Appl. Phys.* **1989**, *22*, 1443–1450.

(19) Johnson, K. L. *Contact Mechanics*; Cambridge University Press: Cambridge, U.K., 1989.

(20) *coblock*(polystyrene-poly(vinylpyridine)) polymer (Polymer Source Inc., Dorval, Canada) was dissolved in THF (2 g/L). Spin casting was performed at 1000 rpm for 2 min using a Headway Research ED101 photoresist spinner. The tip radius was estimated from images obtained on a test object (silicon tip grating, NT-MDT, Moscow, Russia). Indentation data for the sample were collected in 10 mM sodium acetate solution, using a MultiMode AFM (Digital Instruments, Santa Barbara, CA).

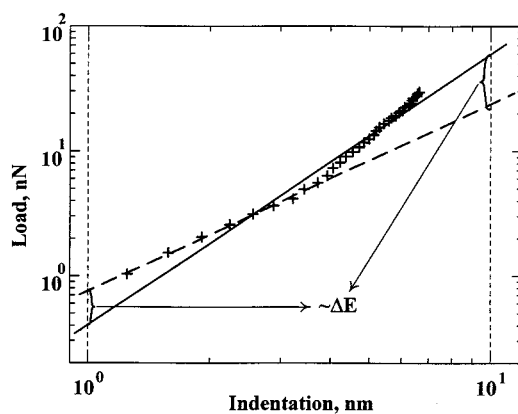


Figure 2. Deviation of load indentation from power law dependence. Force-indentation data were collected on a ~ 30 nm thick spin-cast sample of *coblock*(polystyrene-poly(vinylpyridine)) polymer on a microscope coverslip substrate. The tip radius was approximately 60 nm. Fitting by a straight line in logarithmic coordinates gives the intercept with the ordinate axis. If the intercept is used to determine the Young modulus, the resulting error in the Young modulus will depend on the origin that is chosen for $\log(\delta)$, which is determined by the units of measurement for the indentation δ . Here a solid line is the best linear fit to the force-indentation values that are shown as "+" symbols. The dashed line was calculated according eq 1b with the Young modulus calculated from the data subset with a small a/h ratio. The braces indicate a mismatch in the intercept, which is related to the error in the Young modulus (eqs 2). If the indentation is measured in nanometers, the error will be negative (the brace on the left-hand side). On the other hand, if the indentation is measured in 10 nanometers units for the same set of data, the error will be positive (the brace on the right-hand side).

For this response (non-power-law), Young modulus estimates can have an error that varies with the units of measurements. Indeed, the Young modulus is determined from the intercept of the linear fit line with the ordinate in logarithmic coordinates. Thus, the error depends on the distance between an intercept of the linear fit line in logarithmic coordinates (the ordinate position is determined by $\delta = 1$ unit) and the intercept of the line corresponding to the conditions assumed when deriving eqs 1. Figure 2 illustrates that even the sign of the error changes. Using the units shown in Figure 2, the estimated modulus is two times smaller than when a/h is small.

We have performed numerical calculations that simulate the indentation of an elastic layer bonded to an elastic foundation. Our computations are based on the elastic layer model of Dhaliwal and Rau.²¹ Force-indentation curves are obtained by solving a Fredholm integral equation of the second kind:

$$\phi(t) + \frac{a}{h\pi} \int_0^1 K(x,t)\phi(x) dx = - \frac{Ea}{2(1 - \sigma^2)} \frac{d}{dt} \left[\int_0^t \frac{\delta - f(x)}{\sqrt{t^2 - x^2}} x dx \right] \quad 0 \leq t < 1 \quad (3)$$

Here $K(x,t)$ is the kernel of the integral equation and E and σ are the Young modulus and the Poisson ratio of the layer, respectively. The kernel is defined as

$$K(x,t) = 2 \int_0^\infty H(2u) \cos\left(\frac{a}{h} tu\right) \cos\left(\frac{a}{h} xu\right) du$$

with

(21) Dhaliwal, R. S.; Rau, I. S. *Int. J. Eng. Sci.* **1970**, *8*, 843–856.

$$H(x) = -\frac{b + c(1 + x)^2 + 2bce^{-x}}{e^x + b + c(1 + x^2) + cbe^{-x}}$$

$$b = \frac{(3 - 4\sigma) - \mu(3 - 4\sigma_1)}{1 + \mu(3 - 4\sigma)}$$

$$c = \frac{1 - \mu}{\mu + 3 - 4\sigma}$$

μ is the ratio of Lamé constants²³ with $\mu = (E/2(1 + \sigma))/E_1/2(1 + \sigma_1)$, $f(x)$ in eq 3 is the tip shape function, and here we use the following shapes:²¹

$$f(x) = ax \cot \alpha \quad \text{conical tip}$$

$$f(x) = (a^2/2R)x^2 \quad \text{paraboloidal tip} \quad (4)$$

$$f(x) = R \cot^2 \alpha \sqrt{(ax/R \cot \alpha)^2 + 1 - 1} \quad \text{hyperboloidal tip}$$

where a is the radius of the tip-sample contact area, R is radius of the curvature of the tip apex, and α is the tip semivertical angle as shown in Figure 1.

To find the indentation δ , we use the condition that the normal component of stress remains finite around the circle of contact between the tip and the sample. A solution of (3) must satisfy²¹

$$\phi(1) = 0 \quad (5)$$

We solve eq 3 numerically to determine the indentation. For each value of the contact radius a , we iteratively find the indentation δ such that the solution of (3) satisfies (5), and we find the load force according to²¹

$$F = -4 \int_0^1 \phi(t) dt \quad (6)$$

To estimate the error in the Young modulus unambiguously, we plot logarithmic force-indentation curves in normalized coordinate units:²²

$$\left. \begin{aligned} \tilde{\delta} &= \frac{\delta}{h \cot(\alpha)} \\ \tilde{F} &= \frac{F(1 - \sigma^2)}{2h^2 \cot(\alpha)} \end{aligned} \right\} \text{conical tip} \quad (7a)$$

$$\left. \begin{aligned} \tilde{\delta} &= \frac{\delta \cdot 2R}{h^2} \\ \tilde{F} &= \frac{F \cdot R(1 - \sigma^2)}{h^3} \end{aligned} \right\} \text{paraboloidal tip} \quad (7b)$$

For conical and paraboloidal tips, force vs indentation curves plotted in these coordinates change only when the ratio of Lamé coefficients, μ , changes. μ provides the mismatch between the rigidity moduli of the top layer and the substrate. When $\mu = 1$ and $\sigma = \sigma_1$, the kernel vanishes and eq 3 becomes equivalent to the Abel integral equation considered by Sneddon.¹⁴ The elastic layer indentation curves are not linear in logarithmic coordinates. Therefore, the slope and intercept of straight lines fitted through the data points depend on the maximum indentation value. The Young modulus can be estimated in normalized coordinates using eqs 1a,b, substituting the force and indentation from eqs 7a,b for any maximum indentation value. Hereafter, we use the term Young

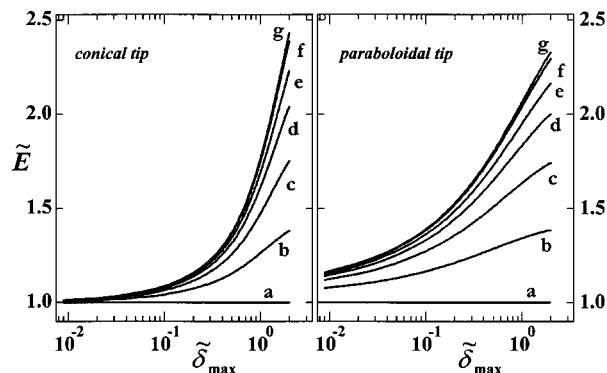


Figure 3. x axis, normalized maximum indentation, plotted against y axis, ratio of Young modulus estimated from linear fit to modulus of top layer: left panel, conical tip; right panel, paraboloidal tip. Different lines correspond to different ratios of Lamé coefficients, and in lines a–g μ corresponds to 1, 0.46, 0.22, 0.1, 0.046, 0.01, and 0.001, respectively.

modulus to indicate the true Young modulus of the top layer material and “estimated Young modulus” to mean that estimated from the linear fit. We calculate the ratio of this estimated Young modulus to the modulus of the top layer (the reduced Young modulus \tilde{E}) and plot it vs the normalized maximum indentation. Plots for different values of μ are shown in Figure 3. The left panel shows the calculated curves for a conical tip, and the right panel shows the calculated curves for a paraboloidal tip. μ values are given in the figure caption. We used equally spaced δ values in our calculations. In the AFM experiment, this is appropriate when the cantilever spring constant is considerably larger than the surface spring constant.

For soft samples, the reduced modulus from Figure 3 can be used as a correction factor to better estimate the Young modulus. When μ is less than 10^{-3} , the lines are almost indistinguishable. Therefore, these lines can be used as correction factors for samples with Young modulus ~ 0.1 GPa and less and for substrates with modulus ~ 100 GPa. For larger values of μ an iterative procedure can be used to correct both E and μ .

As an example, we use the data from Figure 2 to calculate $\tilde{\delta}$ and \tilde{F} according to eq 7b. We take $\sigma = 0.33$ as a reasonable value. The estimated Young modulus is calculated from the intercept of the linear fit in log-log coordinates, according to the equation $E = 3 \exp(b)/\sqrt{2}$, where b is the intercept. Thus we obtain $E = 133$ MPa. The maximum normalized indentation is $\tilde{\delta}_{\max} = 0.88$. Using Figure 3, we conclude that E has been overestimated by a factor ~ 2.1 ; the true modulus is $E = 63$ MPa. This value of the Young modulus is close to the one used to calculate the dashed line in Figure 2, 58 MPa. We note that our indentation values are not equally spaced; this contributes to the inaccuracy in the modulus determination. It is important to know the layer thickness accurately, to determine the correction for E (since normalized indentation in eq 7b is proportional to h^{-2}). If the Young modulus is already known instead, the steep dependence of \tilde{E} on h can be used to estimate the layer thickness.

We have performed an indentation experiment on a poly(vinylpyridine) sample which was spin cast on the surface of microscope coverslip. The sample preparation is described in ref 24. A height image of the sample surface is shown in Figure 4a. Figure 4b shows the force-indentation dependencies for the three locations marked on the image. At these locations, sample thicknesses are 16, 26, and 32 nm. Figure 4c shows the force-indentation dependencies in normalized coordinates calculated using

(22) Rau, I. S.; Dhaliwal, R. S. *Int. J. Eng. Sci.* **1972**, *10*, 659–663.

(23) Landau, L. D.; Lifshitz, E. M. *Elasticity Theory*; Nauka: Moscow, 1987; p 26.

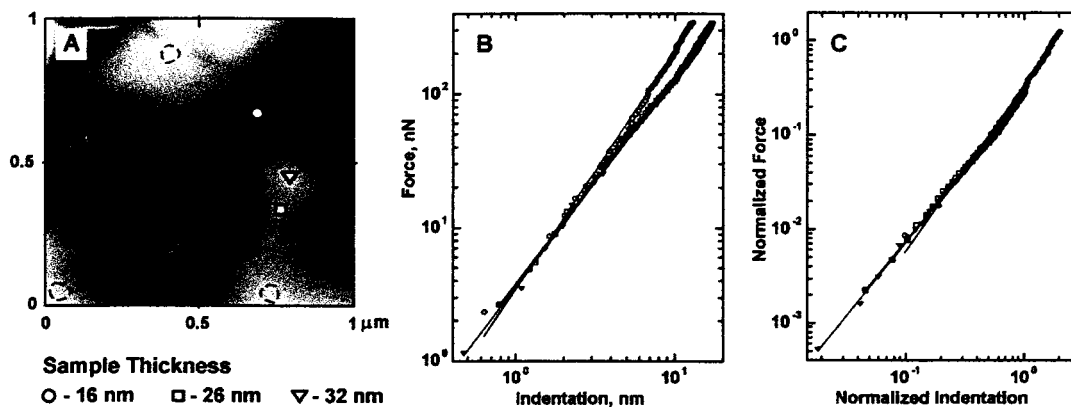


Figure 4. Indentation experiments on a poly(vinylpyridine) polymer sample.²⁴ Panel A contains an intermittent-contact mode image of the sample. Markers indicate positions where the force-indentation data were collected and analyzed. Sample thickness is indicated on the figure. Panel B shows force-indentation dependencies, and panel C shows these dependencies in normalized coordinates. At the marked locations the sample has similar elasticity moduli (0.31, 26, and 0.29 GPa). Because data shown on the plot were collected with the same tip and similar tip-sample interaction geometry, lines coincide on graph C. Markers indicate data collected at three points; solid lines are linear fit lines in logarithmic coordinates. Dashed lines on panel A show areas where additional data analysis was performed (see text).

eq 7b. Uncorrected values of the Young moduli were calculated using eq 1b in normalized coordinates:

$$\tilde{F} = \frac{\sqrt{2}}{3} E \tilde{\delta}$$

The calculated values are 0.72, 0.56, and 0.55 GPa, respectively. When corrected with factors from Figure 3b (line g),²⁵ these values become 0.31, 0.26, and 0.29 GPa, respectively. We note that in our analysis we used data collected on a flat portion of the sample. Data collected on sloped regions could not be corrected using the described procedure. We analyzed force plots collected at 30 different points where the sample thickness varied from 11 to 37 nm. Data collection locations are indicated with dashed lines in Figure 4a. For the uncorrected Young modulus, we obtained a mean value of 0.74 GPa with 0.20 GPa standard deviation and a -0.55 correlation with the sample thickness. The correction²⁵ eliminated this correlation and resulted in a mean value of 0.36 GPa with 0.10 GPa standard deviation. For force plots collected within approximately 60 nm from each other, the width of the distribution is 15% of the mean value. This shows that our poly(vinylpyridine) sample produced by spin casting has noticeable modulus inhomogeneity on a submicrometer scale.

Force-indentation curves for a hyperboloidal tip were transformed according to eq 7b. The results are shown in Figure 5, which gives a plot of the reduced Young modulus vs the maximum normalized indentation, for $\mu \cong 0$ and different $h/(R \cot \alpha)$ ratios. When $h/(R \cot \alpha)$ is small (less

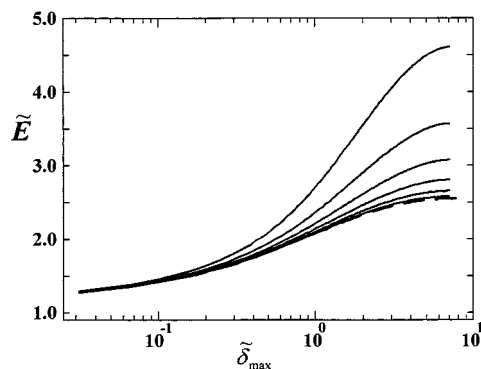


Figure 5. Reduced Young modulus plotted vs normalized maximum indentation for hyperboloidal tip (solid lines). Coordinates were transformed according to the paraboloidal tip eqs 7b. Here $\mu = 0.9 \times 10^{-3}$ and lines (from the top) correspond to $h/(R \cot \alpha)$ ratios of 1.7, 1.2, 0.84, 0.58, 0.36, and 0.18. For comparison we show a calculation for the paraboloidal tip (dashed line).

than 0.1), the hyperboloidal tip indentation curves are close to the paraboloidal tip curve (dashed line). Also, small values of the normalized indentation correspond to a small ratio of maximum contact area radius to layer thickness. In this case, hyperboloidal tip indentation features are similar to paraboloidal tip indentation. Otherwise, hyperboloidal tip indentation cannot be described by simple models and should be treated explicitly.

In addition, the force modulation method can be employed to determine the elasticity of thin layers. In this method, the sample oscillates at a certain frequency. This oscillation is sensed by the tip, which contacts the sample. The amplitude of the tip oscillation depends on sample stiffness, and for a semiinfinite sample, the Young modulus can be estimated using the following equation:

$$E = \sqrt{\frac{[k_c(d/(z-d))]^3}{6RF}} \quad (8)$$

Here k_c is the cantilever spring constant, R is the tip radius of curvature, F is the average load applied to the sample, z is the modulation amplitude of the sample, and d is the tip oscillation amplitude. This equation was derived using Sneddon mechanics for a paraboloidal tip profile, following the approach given in ref 5. For a thin sample, this estimate

(24) Poly(vinylpyridine) polymer with a molecular weight of 50 kDa was purchased from Polymer Source Inc. (Dorval, Canada). The polymer was dissolved in 1,1,1,3,3,3-hexafluoro-2-propanol (Aldrich) (1 g/L). Samples were spin cast on microscope cover glass (Fisher Scientific) at 4000 rpm for 1.5 min using a Headway Research ED101 photoresist spinner. The tip radius was estimated from images obtained on a test object (silicon tip grating, NT-MDT, Moscow, Russia). The cantilever spring constant was measured using force calibration cantilevers with a known spring constant (Park Scientific Instruments, Sunnyvale, CA). Indentation data for the sample were collected in 25 mM sodium acetate solution, using a MultiMode AFM (Digital Instruments, Santa Barbara, CA).

(25) For convenience, we approximated correction coefficients for the soft top layer and paraboloidal tip shape using the function $\log(\tilde{E} - 1) = P(\log(\tilde{\delta}_{\max}))$, where $P(x)$ is a 3rd order polynomial with coefficients $\{-0.008\ 042\ 4, -0.060\ 512, 0.349\ 233, 0.067\ 542\}$ in decreasing power order. This function gives correction coefficients with 1% accuracy for maximum normalized indentation in the range from 10^{-2} to 5.

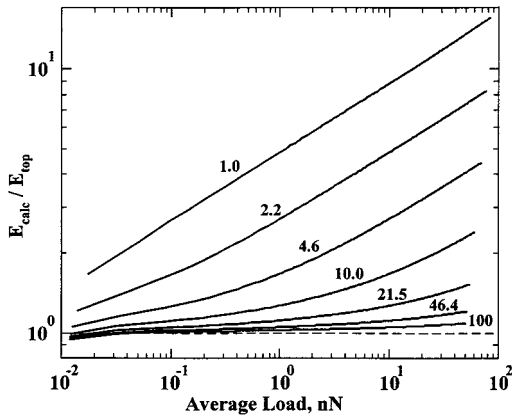


Figure 6. Ratio of the modulus estimated using eq 8 to the actual value given as function of average load for samples of different thickness. Different lines correspond to different layer thicknesses. The thickness (from 1 to 100 nm) is indicated on the graph. Other parameters: tip radius of curvature 10 nm; $\mu = 0.01$; $E = 1$ GPa; $\sigma = 0$; $k_c = 10$ N/m; sample oscillation amplitude 0.02 nm.

can result in substantial error. Figure 6 shows the reduced Young modulus (estimated according to eq 8) vs the applied load for samples of different thickness. The parameters are given in the figure caption. Figure 6 demonstrates that a change in the sample thickness may result in an apparent softness contrast in the force–modulation images.

Figure 7 shows the same dependence as Figure 6, where the lines are calculated in normalized coordinates using eqs 7b and 8 for several values of μ . When the layer thickness, tip radius, and elastic parameters of substrate (E_1 , σ_1) are known and a reasonable assumption about the Poisson ratio of the elastic layer can be made, the reduced elastic modulus can be used to correct the error in the measured modulus. Since we do not know a priori the correct value of μ (it depends on the true Young modulus), an iterative procedure can be employed to determine the correction coefficient. Let E^* be the symbol for the Young modulus, as estimated from eq 8. To obtain the correction factor for E^* , the corresponding average normalized load can be obtained from eq 7b. This gives a fixed position on the abscissa of Figure 7. The ratio of E^* to the Young modulus of substrate (E_1) gives an approximate value of μ . From Figure 7, an approximate correction factor \bar{E} can be found; from this we can find a better estimate for $\mu = E^*/(\bar{E}E_1)$. This gives an adjusted correction factor \bar{E} . This then improves the estimate of μ . The iterations converge in a few steps to a best value of μ , resulting in a correction factor for E^* . As an example,

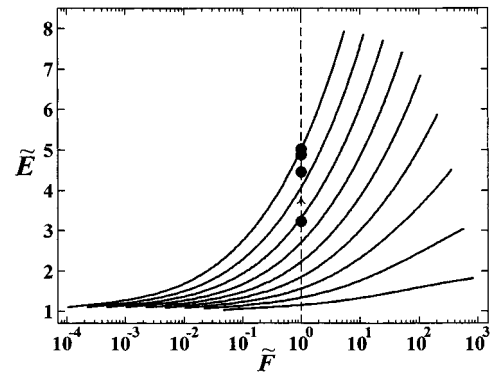


Figure 7. Plots of the reduced modulus vs the normalized force for different μ values illustrating a possible error in the Young modulus as determined using the force–modulation technique. μ , starting from the top: 0.001, 0.0022, 0.0046, 0.01, 0.022, 0.046, 0.1, 0.22, and 0.46. Circles show an iterative process to determine the correction factor for the estimated Young modulus.

we consider $E^* = 0.5$ GPa, $E_1 = 100$ GPa, and $\bar{F} = 1$. The iterative process using these parameters is represented by circles in Figure 7. Initially, $\mu \gg 0.005$. From the figure, we can see that for this μ , $\bar{E} \approx 3$. This decreases the estimate of μ to 0.0016, giving us $\bar{E} \approx 4.5$. The next step results in $\bar{E} \approx 5$, and subsequent iterations do not change the correction factor significantly. Thus, we conclude that the true elastic modulus is close to 0.1 GPa.

To summarize, we have modeled an elastic layer on an elastic foundation and found an error associated with using an elastic half-space model to estimate the Young modulus via AFM indentation and force–modulation experiments. We find that the application of semiinfinite sample models can result in unpredictable and significant errors in Young modulus estimates. Normalized coordinates should be used to obtain consistent results. Contrast in the force–modulation imaging may be related to inhomogeneities in the sample thickness. We have proposed a method to reduce the error related to finite sample thickness. Elasticity characterization of layered, thin, or composite samples can benefit from the described method.

Acknowledgment. We gratefully acknowledge the ONR (Grant N0001-96-1-0735) for financial support. B.B.A. gratefully acknowledges the Mellon Foundation for a predoctoral fellowship. G.C.W. gratefully acknowledges 3M Co. for an Untenured Faculty Award. We also thank Jason Bemis for the poly(vinylpyridine)–polystyrene data.

LA980585Z